CONVECTIVE CHARACTERISTICS AND GOES-16 GLM OPTICAL ENERGY IN HURRICANE IAN (2022)

Kiahna Mollette*, Patrick Duran, Christopher Schultz
NASA, Marshall Space Flight Center

1. INTRODUCTION

Tropical cyclone (TC) track forecasts have improved greatly in recent decades, while intensity forecasts have struggled to improve at the same rate. As a result, there has been a focus in literature to attempt to better understand the processes that lead to TC intensification and especially TC rapid intensification (RI). Lightning has been studied as a tool to determine changes in TC intensity, but studied thus far have had conflicting results.

DeMaria et al. (2012) and Stevenson et al. (2016) found that an increase in inner core lightning flashes may indicate imminent TC weakening while increases in outer band flash rate may indicate imminent TC intensification. This differs from multiple studies that found that an increase in inner core flash rates has been shown to occur just prior to TC intensification (Molinari et al. 1994, 1999; Fierro et al. 2011; Zhang et al. 2015; Stevenson et al. 2014, 2018; Duran et al. 2021). These inconsistencies indicate that the physical processes that lead to changes in flash rates are not well understood in the inner core of TCs.

In order for electrification to occur, there need to be updrafts sufficient of elevating hydrometeors through the mixed phase region, from approximately 0 to -40 degrees Celsius. An increase in updrafts also contributes to increases in TC intensity, which may allow for a relationship to be drawn between TC intensification and lightning behavior. This paper investigates and compares convective characteristics and lightning behavior in the innermost 100 km during two rapid intensification period in Hurricane Ian (2022). It hypothesizes that the same updrafts that contribute to TC RI are lofting hydrometeors through the mixed phase region as well as around and outward from the eye as a result of the TC primary and secondary circulation. This allows for a larger area of electrified hydrometeors and provides an environment that would allow for larger and brighter flashes to occur.

2. DATA & METHODOLOGY

2.1. GOES-16 GLM

The Geostationary Operational Environmental Satellites-16 (GOES-16) Geostationary Lightning Mapper (GLM) provides not only higher detection efficiency than many ground-based lightning detection networks, but it also provides flash energy and area along with flash density. GLM measures lightning using an optical imager on a sub-minute scale, meaning that there are near-constant observations of lightning in a TC (Goodman et al. 2013). This can provide information about TC behavior on a very small temporal scale, allowing for the analysis of rapid changes.

This paper utilizes the GOES-16 GLM optical energy measurements to examine changes in flash energy during both RI periods in Ian.

2.2. NOAA TDR

The National Oceanic and Atmospheric Administration (NOAA) conducts flights into TCs in order to collect crucial data that may help scientists to better understand how a TC may be changing. The WP-3D (P-3) aircraft make flights through the center of the TC while utilizing multiple radars to measure quantities such as reflectivity and vertical velocity. The tail Doppler radar (TDR) is a vertically scanning radar which allows for an analysis of the storm using vertical and horizontal cross-sections.

This study utilizes the vertical velocity measurements from the TDR to calculate the updraft volume through both RI periods. Basarab et al. (2015) found that flash rates could be associated with the graupel volume, 35 dBZ volume, and the 5 m/s updraft volumes. Black et al. (1996) found using airborne radar measurements that less than 5% of updrafts in TCs reach 5 m/s, which explains why lightning is much less frequent in TCs than mid-latitude thunderstorms. Despite their rarity, the 5 m/s updrafts may provide a basis for determining if a TC is producing updrafts capable of transporting hydrometeors through the mixed phase region. As a result, the volume of these updrafts is calculated for this paper.

The TDR reflectivity is utilized in this paper to calculate the mass of ice in the the mixed phase region. This is made possible by a multitude of measurements and calculations derived utilizing direct measurements of hydrometeor concentrations and size in clouds. Heymsfield and Miller (1988) derived equations from measurements in mid-latitude thunderstorms, producing equations to calculate the ice water content (IWC) in thunderstorms. Black (1990) further iterated on these equations, instead using measurements from TC convective and stratiform clouds. Given that the clouds in a TC vary between convective and stratiform in nature, the equation produced that includes measurements from both types of clouds is utilized in this paper:

$$Z = 670 * (IWC)^{1.51} \tag{1}$$

This can be rearranged in order to calculate the ice mass from the measured reflectivity. The IWC will then be multiplied by the grid size (2000m x 2000m x 500m) in order to produce the ice mass in kg:

* *Corresponding author address:* 320 Sparkman Dr NW, Huntsville, AL 35805;
E-mail: kiahna.r.mollette@nasa.gov.

$$m_{ice} = (2.64 * 10^{-2} Z^{0.5587}) * (2000 * 2000 * 500) * 10^{-3} \quad (2)$$

The GLM flash energy, TDR 5 m/s updraft volume, and ice mass will all be investigated during the first and second RI periods in Hurricane Ian and compared to determine if there are physical differences as determined by the TDR measurements that may correlate with differences in flash energy and flash rate. The TDR derived convective characteristics will be determined from the downshear left quadrant as determined by the Statistical Hurricane Intensity Prediction Scheme (SHIPS). This is to account for differences in swath directions and differences in TC structure in different shear quadrants.

3. RESULTS

Plots displaying the evolution of TC intensity, GLM optical energy and flash rates, and TDR derived ice mass and 5 m/s updraft volume were created to analyze how these variables change through time (Fig. 1). The first RI period, highlighted in yellow, displays the lack of lightning within this time (Fig. 1b). This is indicated by the infrequent occurrence of optical energy being measured. Conversely, the second RI period, highlighted in blue, experienced near-constant lightning with varying flash rates throughout this period (Fig. 1b). During the second RI period, the optical energy per flash increases steadily while the flash rates do not increase at the same rate. The flash rates only peak at the end of RI, which supports previous literature that showed a peak in lightning flash rate at the end of an intensification period (Molinari et al. 1999).

The ice mass is calculated using Eq. 2 utilizing the TDR reflectivity. It slowly increases through time from the beginning of the first RI period until the end of the second RI period, increasing from approximately $5 * 10^8$ kg to $2 * 10^9$ kg (Fig. 1c). The volume of the 5 m/s updraft volume stays relatively similar between the two RI periods, with a large peak in the final swath at the end of the second RI period (Fig. 1c).

Investigating these variables further, the reflectivity and vertical velocity swaths are plotted as well as the difference between them. The difference is calculated by subtracting the values from the first RI from the second RI only using grid points where they overlap. The reflectivity is plotted at the 10 km level as this is likely representing frozen hydrometeors as it is near the top of the mixed phase region as determined by dropsonde measurements. The reflectivity during both RI periods is plotted (Fig. 2 a-f) as well as the difference, with a positive difference shown around the eye in all three compared swaths (Fig. 2 g-i).

The vertical velocity difference is plotted for both RI periods at 5 km (Fig. 3 a-f). The plots show the vertical velocity at 5 km because updrafts at the bottom of the mixed phase region need to be strong enough to loft hydrometeors into the mixed phase region in order for some of these particles to freeze and become electrified. The difference plots are again created by subtracting values from the first RI from the second RI to determine if the vertical velocity increased or decreased between the two RI periods. The difference plots indicate that there are increased updraft volumes around the eye in all three swaths, and overall very few areas of decreased vertical velocity (Fig. 3 g-i).

4. DISCUSSION & CONCLUSIONS

Fig. 2 and Fig. 3 are supportive of the hypothesis that increases in updrafts and reflectivity may be what allows for an electrically active inner core and may assist in justifying the contrasting behavior between the two RI periods in Ian.

While Fig. 1c indicates very little change in the 5 m/s updraft volume between the two RI periods, the two periods exhibit unique updraft behaviors. The first RI period experienced many small updraft cores while the second RI period has fewer but much larger updraft cores. Small and separate updrafts may explain the lack of lightning in the first RI period as the updrafts being disconnected can lead to a couple of limiting factors: the lightning may not be able to propagate very far as the electrified particles may not extend very far outside of the updrafts and there may not be enough electrified hydrometeors to initiate lightning in small updrafts. The second RI period, having fewer but contiguous updrafts, allows for a larger area for the electrified hydrometeors to propagate to and therefore provides an environment more supportive of larger and brighter lightning.

This work provides an analysis of the convective characteristics and GLM optical energy in Hurricane Ian (2022) and finds that the shape and volume of the 5 m/s updrafts as well as the ice mass in the mixed phase region may impact TC electrification in the inner core.

Acknowledgments. Funding for this work was provided by the NASA Pathways Program and directed support to the Short-Term Prediction Research and Transition (SPoRT) Center from Dr. Tsengdar Lee at NASA HQ.

REFERENCES

Basarab, B. M., S. A. Rutledge, and B. R. Fuchs, 2015: An Improved Lightning Flash Rate Parameterization Developed from Colorado DC3 Thunderstorm Data for Use in Cloud-Resolving Chemical Transport Models. *Journal of Geophysical Research: Atmospheres*, **120**, 9481–9499, doi:10.1002/2015JD023470.

Black, M. L., R. W. Burpee, and F. D. M. Jr., 1996: Vertical Motion Characteristics of Tropical Cyclones Determined with Airborne Doppler Radial Velocities. *Journal of the Atmospheric Sciences*, **53**, 1887–1909, doi:10.1175/1520-0469(1996)053<1887:VMCOTC>2.0.CO;2.

Black, R. A., 1990: Radar Reflectivity-Ice Water Content Relationships for Use above the Melting Level in Hurricanes. *Journal of the Applied Meteorology*, **29**, 955–961,

DeMaria, M., R. T. DeMaria, J. A. Knaff, and D. Molenar, 2012: Tropical Cyclone Lightning and Rapid Intensity Change. *Monthly Weather Review*, **140**, 1828–1842, doi:10.1175/MWR-D-11-00236.1.

Duran, P., and Coauthors, 2021: The Evolution of Lightning Flash Density, Flash Size, and Flash Energy During Hurricane Dorian's (2019) Intensification and Weakening. *Geophysical Research Letters*, **48**, 1–11, doi:10.1029/2020GL092067.

Fierro, A. O., X.-M. Shao, T. Hamlin, J. M. Reisner, and J. Harlin, 2011: Evolution of Eyewall Convective Events as Indicated by Intracloud and Cloud-to-Ground Lightning Activity during the Rapid Intensification of Hurricanes Rita and Katrina. *Monthly Weather Review*, **139**, 1492–1504, doi:10.1175/2010MWR3532.1.

Goodman, S. J., and Coauthors, 2013: The GOES-R Geostationary Lightning Mapper (GLM). *Atmospheric Research*, **125-126**, 34–49, doi:10.1016/j.atmosres.2013.01.006.

Heymsfield, A. J., and K. M. Miller, 1988: Water Vapor and Ice Mass Transported into the Anvils of CCOPE Thunderstorms: Comparison with Storm Influx and Rainout. *Journal of the Atmospheric Sciences*, **45**, 3501–3514,

Molinari, J., P. Moore, and V. Idone, 1999: Convective Structure of Hurricanes as Revealed by Lightning Locations. *Monthly Weather Review*, **127**, 1828–1842, doi:10.1175/1520-0493.

Molinari, J., P. Moore, V. Idone, R. W. Henderson, and A. B. Saljoughy, 1994: Cloud-to-ground lightning in Hurricane Andrew. *Journal of Geophysical Research*, **99**, 16 665–16 676, doi:10.1029/94JD00722.

Stevenson, S. N., K. L. Corbosiero, and S. F. Abarca, 2016: Lightning in Eastern North Pacific Tropical Cyclones: A Comparison to the North Atlantic. *Monthly Weather Review*, **144**, 225–239, doi:10.1175/MWR-D-15-0276.1.

Stevenson, S. N., K. L. Corbosiero, M. DeMaria, and J. L. Vigh, 2018: A 10-Year Survey of Tropical Cyclone Inner-Core Lightning Bursts and Their Relationship to Intensity Change. *Weather and Forecasting*, **33**, 23–36, doi:10.1175/WAF-D-17-0096.1.

Stevenson, S. N., K. L. Corbosiero, and J. Molinari, 2014: The Convective Evolution and Rapid Intensification of Hurricane Earl (2010). *Monthly Weather Review*, **142**, 4364–4380, doi:10.1175/MWR-D-14-00078.1.

Zhang, W., Y. Zhang, D. Zheng, F. Wang, and L. Xu, 2015: Relationship between Lightning Activity and Tropical Cyclone Intensity over the Northwest Pacific. *Journal of Geophysical Research: Atmospheres*, **120**, 4072–4089, doi:10.1002/2014JD022334.

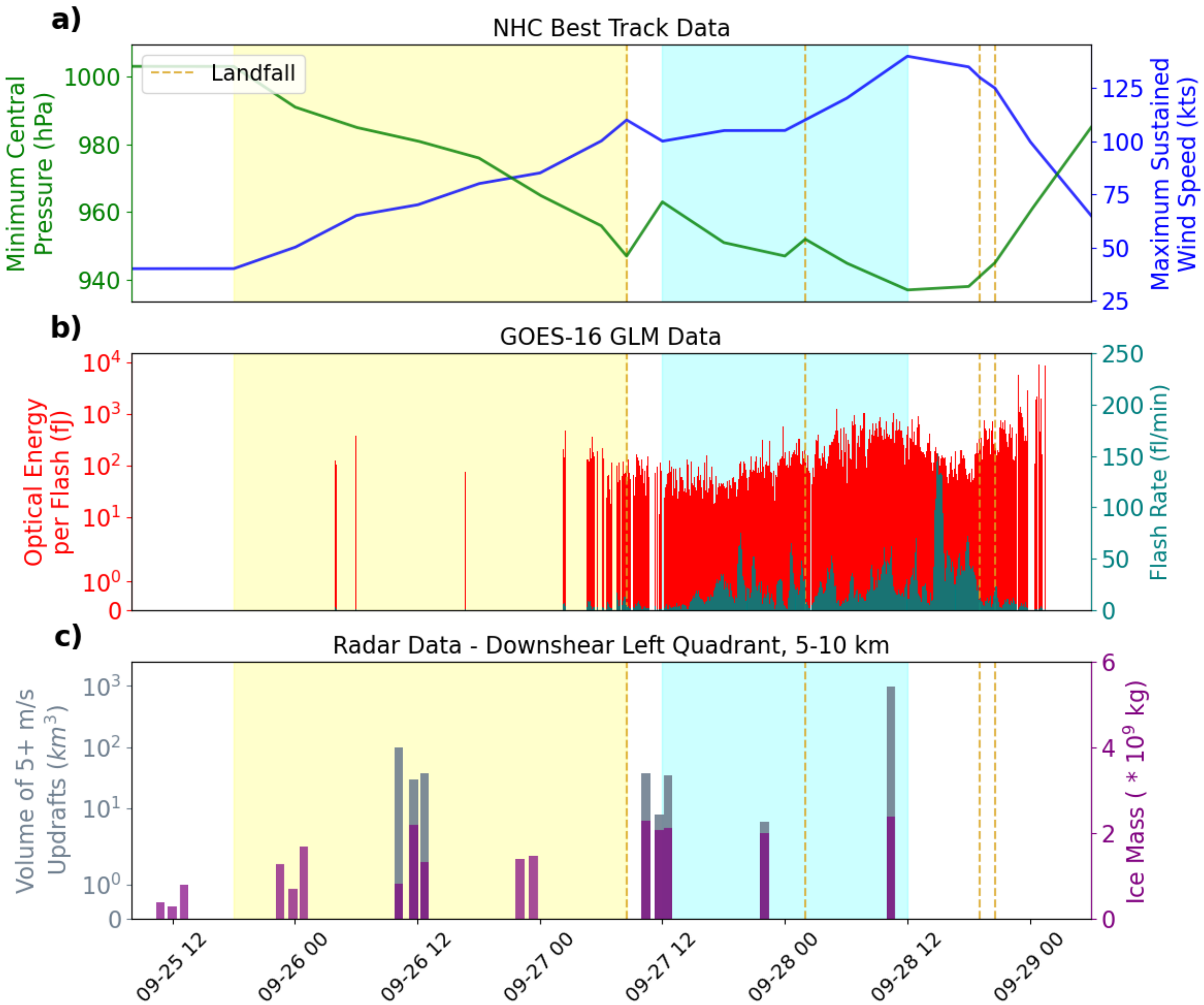

FIG. 1. (a) NHC Best Track minimum central pressure (green) and maximum sustained wind speeds (blue). (b) GOES-16 GLM optical energy per flash (red) and flash count (teal). The optical energy per flash is on a logarithmic scale. (c) Convective characteristics as calculated from the NOAA P-3 tail Doppler radar flight volume of the 5+ m/s updrafts (gray) and ice mass (purple). The first RI period is highlighted in yellow, the second RI period is highlighted in cyan, and each landfall is marked with a vertical dashed yellow line.

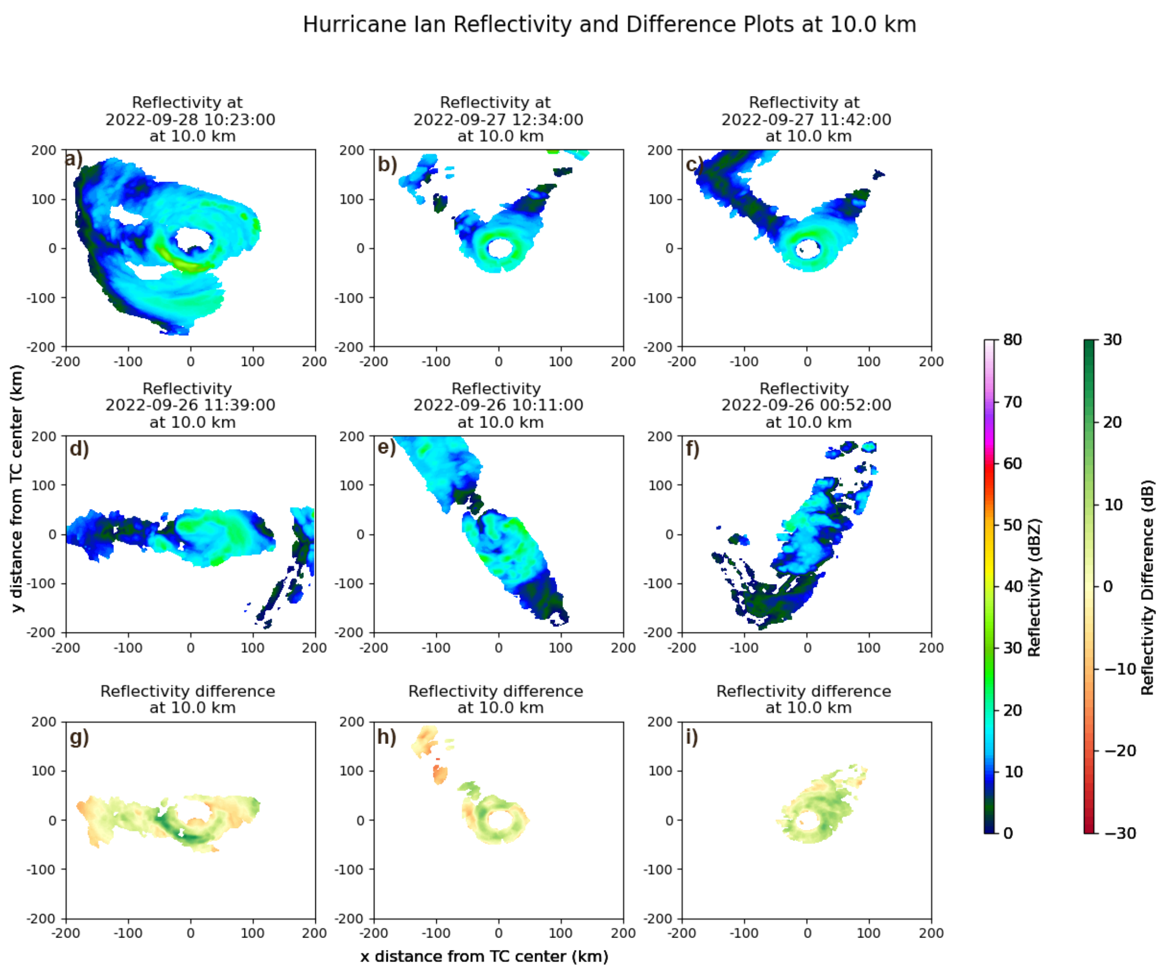

FIG. 2. (a-c) TDR reflectivity during the second RI period. (d-f) TDR reflectivity during the first RI period. (g-i) TDR reflectivity from the first RI subtracted from the reflectivity from the second RI.

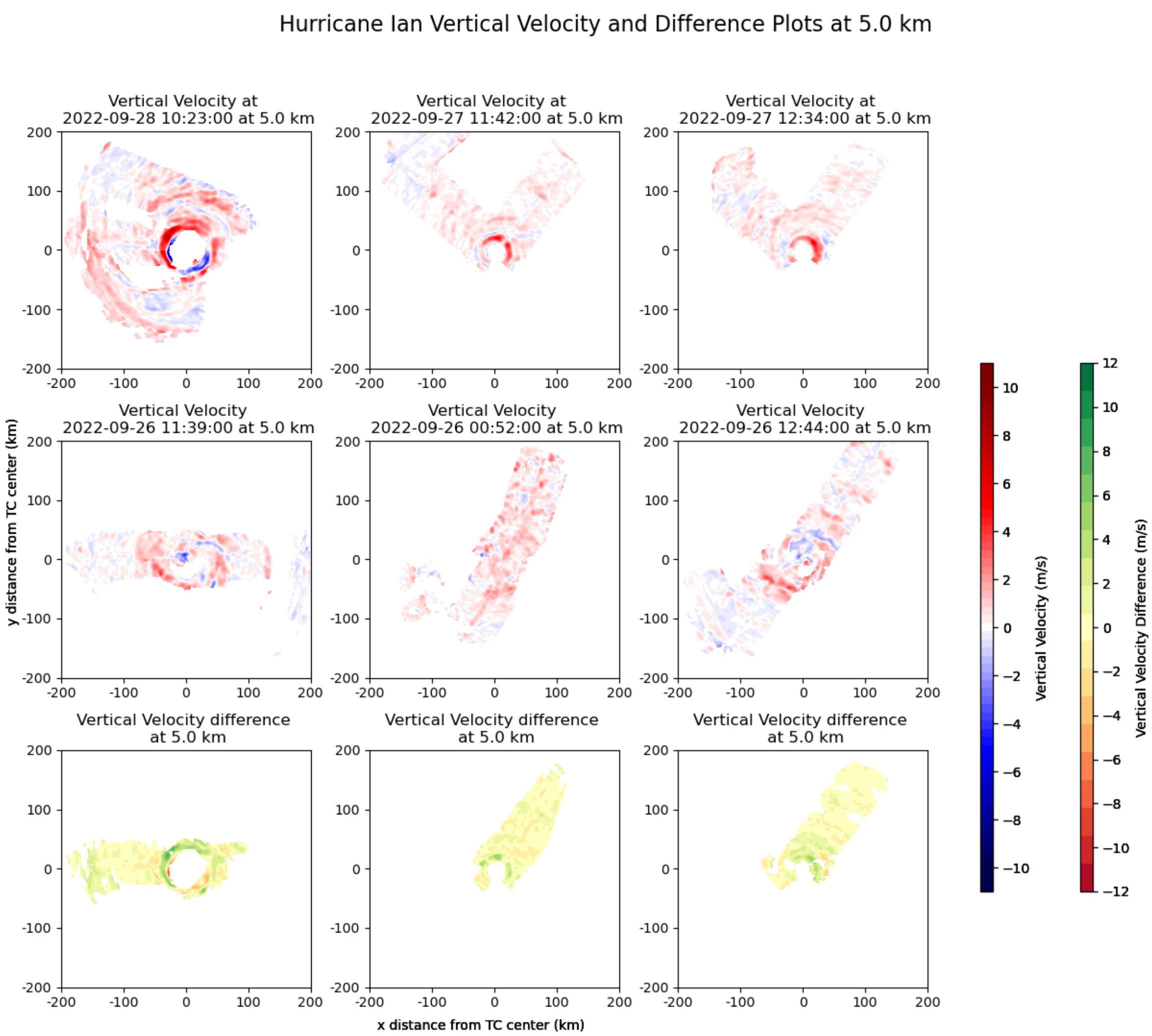

FIG. 3. (a-c) TDR vertical velocity during the second RI period. (d-f) TDR vertical velocity during the first RI period. (g-i) TDR vertical velocity from the first RI subtracted from the vertical velocity from the second RI.